A time-modulated Hawkes process to model the spread of COVID-19 and the impact of countermeasures

(Article begins on next page)

23 April 2024

A time-modulated Hawkes process to model the spread of COVID-19 and the impact of countermeasures[⋆]

Michele Garetto[a,*], Emilio Leonardi[b], Giovanni Luca Torrisi[c]

[a]*Università degli Studi di Torino, C.so Svizzera 185, Torino, Italy*
[b]*Politecnico di Torino, C.so Duca degli Abruzzi 24, Torino, Italy*
[c]*IAC-CNR, Via dei Taurini 19, Roma, Italy*

Abstract

Motivated by the recent outbreak of coronavirus (COVID-19), we propose a stochastic model of epidemic temporal growth and mitigation based on a time-modulated Hawkes process. The model is sufficiently rich to incorporate specific characteristics of the novel coronavirus, to capture the impact of undetected, asymptomatic and super-diffusive individuals, and especially to take into account time-varying counter-measures and detection efforts. Yet, it is simple enough to allow scalable and efficient computation of the temporal evolution of the epidemic, and exploration of what-if scenarios. Compared to traditional compartmental models, our approach allows a more faithful description of virus specific features, such as distributions for the time spent in stages, which is crucial when the time-scale of control (e.g., mobility restrictions) is comparable to the lifetime of a single infection. We apply the model to the first and second wave of COVID-19 in Italy, shedding light onto several effects related to mobility restrictions introduced by the government, and to the effectiveness of contact tracing and mass testing performed by the national health service.

Keywords: COVID-19, Compartmental models, Branching process, Hawkes process

1. Introduction and related work

Models of epidemic propagation are especially useful when they provide key insights while retaining simplicity and generality. For example, in mathematical epidemiology the SIR model reveals in very simple terms the fundamental role of the basic reproduction number (R_0) which governs the macroscopic, long-term evolution of the outbreak in a homogeneous population. The vast majority of models developed for the novel SARS-CoV-2 are extensions to the classic SIR, along the standard approach of introducing additional compartments to describe different phases of the infection, the presence of asymptomatic, symptomatic or pauci-symptomatic individuals, the set of quarantined, hospitalized people, and so on. Such models lead to a system of coupled ODE's with fixed or time-varying coefficients to be estimated from traces. A very incomplete list of modeling efforts pursued in this direction, early applied to COVID-19, includes the SEIR models in [1, 2, 3, 4, 5], the SIRD models in [6, 7], the SEPIA model in [8], the SIDHARTE model in [9].

In this paper we adopt a different approach that allows a more accurate representation of native characteristics of a specific virus, such as actual distributions of the duration of incubation, pre-symptomatic and symptomatic phases, for various categories of infected. This level of detail is important when the intensity of applied countermeasures varies significantly over time-scales comparable to that of an individual infection, and we believe it is essential to address fundamental questions such as: i) when and to what extent can we expect to see the effect of specific mobility restrictions introduced by a national government at a given point in time? ii) what is the impact of hard vs partial lockdowns enforced for given numbers of days? when can restrictions be safely released to restart economic and social activities while still keeping the epidemic under control?

Specifically, we propose and analyse a novel, modulated version of the marked Hawkes process, a self-exciting stochastic point process with roots in geophysics

and finance [10]. In a nutshell, in the standard marked Hawkes process each event i with mark m_i, occurring at time t_i, generates new events with stochastic intensity $\nu(t - t_i, m_i)$, where $\nu(\cdot, m_i)$ is a generic kernel. The process unfolds through successive generations of events, starting from so-called immigrants (generation zero). In our model events represent individual infections, and a modulating function $\mu(t)$, which scales the overall intensity of the process at real time t, allows us to take into account the impact of time-varying mobility restrictions and social distance limitations. In addition, we model the transition of infected, undetected individuals to a quarantined state at inhomogeneous rate $\rho(t)$, to describe the time-varying effectiveness of contact tracing and mass testing.

We mention that branching processes of various kind, including Hawkes processes, have been proposed in various biological contexts [11, 12, 13, 14], [15, 16, 17, 18, 19, 20]. In particular [16, 17, 18] propose stationary and non-stationary Hawkes models (i.e., Hawkes processes with time-varying kernels) to model the outbreak of several epidemics, such as Ebola and COVID-19. In [19] authors proposed a first comparison of SIR, SEIR, and Hawkes (with Gamma or Weibull kernels) to forecast the spread of COVID-19. In [20] a comparison between SEIR and Hawkes (with a non-parametric estimate of the kernel) was done for the Ebola outbreak in West Africa. The authors show that, in general, Hawkes predictions are more accurate, leading to lower root mean square errors (RMSE). With respect to previous models based on Hawkes processes, the main novelty of our approach is the use of a *marked* Hawkes process, where the mark encodes different classes of infected and variable durations of stages, together with the application of a *continuous* modulating function to the conditional process intensity.

In [21], a probabilistic extension of (deterministic) discrete-time SEIR models, based on multi-type branching processes, has been recently applied to COVID-19 to capture the impact of detailed distributions of the time spent in different phases, together with mobility restrictions and contact tracing. Another work that, similarly to ours, stresses the importance of handling pre-

3

cise delay distributions is [22], where authors develop a non-Markovian age-of-infection model of the COVID-19 epidemic in Illinois, which can be regarded as a deterministic mean-field approximation of an Hawkes process. In parallel to us, authors of [23] have proposed a Hawkes process with spatio-temporal "covariates" for modeling COVID-19 in the US, together with an EM algorithm for parameter inference. The work in [23] is somehow orthogonal to us, since they focus on spatial and demographic features, aiming at predicting the trend of confirmed cases and deaths in each county. In contrast, we introduce marks and stages to natively model the course of an infection for different categories of individuals, with the fundamental distinction between real and detected cases. Moreover, we take into account the impact of time-varying detection efforts and contact tracing. At last, we obtain analytical expressions for the first two moments of the number of individuals who have been infected within a given time. We mention that, using a radically different approach, machine learning techniques have recently been proposed to describe the intensity of general temporal point processes [24], and they have also been applied to estimate COVID-19 epidemiological curves [25].

We demonstrate the applicability of our model to the novel COVID-19 pandemic by considering real traces related to the first and second wave of coronavirus in Italy. Our fitting exercise, though largely preliminary and based on incomplete information, suggests that our approach has good potential and can be effectively used both for planning counter-measures and to provide an a-posteriori explanation of observed epidemiological curves.

The paper is organized as follows. In Sec. 2 we provide the mathematical formulation of the proposed modulated Hawkes process to describe the temporal evolution of the epidemic. In Sec. 3 we motivate our approach by comparing it to the standard SIR model. Some mathematical results related to the moment generating function of our process are presented in Sec. 4. In Sec. 5 we describe our COVID-19 model based on the proposed approach. We separately fit our model to the first and second wave of COVID-19 in Italy in Sec. 6 and 7, respectively, offering hopefully interesting insights about what happened in this

4

country (and similarly in other European countries) during the recent pandemic. We conclude in Sec. 8.

2. Mathematical formulation of modulated Hawkes process

We first briefly recall the classic Hawkes process restricted to the temporal dimension (the spatio-temporal formulation is similar, but we focus in this work on the purely temporal version). Events of the process (or points) occur at times $T = \{T_i\}_{i \geq 1}$, which are $\mathbb{R}$-valued random variables. A subset I of these points, called immigrants, are produced by an inhomogeneous Poisson process of given intensity $\sigma(t)$. Each immigrant, independently of others, is the originator of a progeny (or cluster) of other points, dispersed in the future through a self-similar branching structure: a first generation of points is produced with intensity $\nu(t - T_j)$, where T_j is the occurrence time of immigrant j, and $\nu : \mathbb{R}^+ \to \mathbb{R}^+$ is a kernel function. Each point of the first generation, in turn, generates new offsprings in a similar fashion, creating the second generation of points, and so on.

The above process can be easily extended to account for different types of points with type-specific kernel functions. Types are denoted by marks $M = \{M_i\}_{i \geq 1}$, which are assumed to be i.i.d. random variables with values on an arbitrary measurable space $(\mathrm{M}, \mathcal{M})$, with a probability distribution $\mathbb{Q}$. Let $N(t, m)$ be the counting process associated to the marked points $N = \{(T_i, M_i)\}_{i \geq 1}$. The (conditional) stochastic intensity $\lambda(t)$ of the overall process is then given by:

$$\lambda(t) = \sigma(t) + \int_0^t \nu(t - s, m) N(\,\mathrm{d}s,\,\mathrm{d}m) = \sigma(t) + \sum_{T_k \cap (0,t)} \nu(t - T_k, M_k)$$

where $\nu : \mathbb{R}^+ \times \mathrm{M} \to \mathbb{R}^+$ is a type-dependent kernel function. In the following we assume $\overline{\nu}(t) := \mathbb{E}[\nu(t, M_1)]$ to be summable,. i.e.

$$R_0 = \int_0^\infty \overline{\nu}(t)\mathrm{d}t < \infty \tag{1}$$

Note that R_0 is the average number of offsprings generated by each point, which is usually referred to as basic reproduction number in epidemiology. The process is called subcritical if $R_0 < 1$, supercritical if $R_0 > 1$.

Our main modification to the above classic marked Hawkes process N is to modulate the instantaneous generation rate of offsprings $N' = N \setminus I$ by a positive, bounded function $\mu(t) : \mathbb{R}^+ \to \mathbb{R}^+$, representing the impact of mobility restriction countermeasures[1]

By so doing, we obtain the modified stochastic intensity of the process:

$$
\begin{aligned}
\lambda(t) &= \sigma(t) + \mu(t) \left[\int_0^t \nu(t - s, m) N(\,\mathrm{d}s,\ \mathrm{d}m) \right] \\
&= \sigma(t) + \mu(t) \left[\sum_{T_k \in (0,t)} \nu(t - T_k, M_k) \right]
\end{aligned}
\tag{2}
$$

Note that, when $\mu(t) = \mu$ is constant, we re-obtain a classic Hawkes process with modified kernel $\mu\,\nu()$. In general, the obtained process is no longer self-similar. In particular, the average number of offsprings generated by a point becomes a function of time:

$$
R(t) = \int_0^\infty \mu(t + \tau) \overline{\nu}(\tau) \, \mathrm{d}\tau
\tag{3}
$$

which provides the infamous real-time reproduction number usually referred to on the media as 'Rt index'.

We emphasize that the process can initially start in the supercritical regime, and then it can become subcritical for effect of a decreasing function $\mu()$, a case of special interest in our application to waves of COVID-19. We mention that the great bulk of literature related to the Hawkes process and its applications to geophysics and finance focuses on the subcritical regime, whereas our formulation applies also to the supercritical regime, which is more germane to epidemics.

---

[1]In this paper, we will call for simplicity 'mobility restrictions' all forms of non-pharmaceutical interventions affecting the virus transmission, such as stay-at-home orders, closures of bars and restaurants, mask mandates, and other governmental policies.

The conditional intensity (2) can be easily de-conditioned with respect to N, obtaining the 'average' stochastic intensity $\overline{\lambda}(t) := \mathbb{E}[\lambda(t)]$:

$$
\begin{aligned}
\overline{\lambda}(t) &= \sigma(t) + \mu(t)\mathbb{E}\left[\int_{(0,t)\times M} \nu(t-s,m)N(\mathrm{d}s,\mathrm{d}m)\right]\\
&= \sigma(t) + \mu(t)\mathbb{E}\left[\int_{(0,t)\times M} \nu(t-s,m)\lambda(s)\,\mathrm{d}s\mathbb{Q}(\mathrm{d}m)\right]\\
&= \sigma(t) + \mu(t)\mathbb{E}\left[\int_0^t \overline{\nu}(t-s)\lambda(s)\mathrm{d}s\right]\\
&= \sigma(t) + \mu(t)\int_0^t \overline{\nu}(t-s)\overline{\lambda}(s)\mathrm{d}s.
\end{aligned}
\tag{4}
$$

where we recall that $\overline{\nu}(t) = \mathbb{E}[\nu(t,M_1)]$.

We observe that (4) is a linear Volterra equation of the second kind, which can be efficiently solved numerically.[2] In the special case of constant modulating function, (4) reduces to a convolution equation which can be analyzed and solved by means of Laplace transform techniques (see Appendix A).

At last we introduce the total number of points up to time t, $N(t)$ (regardless of their associated marks), and its average:

$$
\overline{N}(t) = \int_0^t \overline{\lambda}(\tau)\,\mathrm{d}\tau
\tag{5}
$$

3. Comparison with SIR model

When the kernel function has an exponential shape, i.e., $\nu(t) = Ke^{-\gamma t}$, it is possible to establish a simple connection between the Hawkes process and the classic SIR model [26]. Specifically, consider a stochastic SIR model with an infinite population of susceptible individuals, where each infected generates new infections at rate β, and recovers at rate γ (i.e., after an exponentially distributed amount of time of mean $1/\gamma$). Then the average intensity of the process generated by this stochastic SIR, averaging out the times at which nodes recover, has exactly the (conditional) intensity of a Hawkes process starting

---

[2]For example, the standard trapezoidal rule allows obtaining a discretized version of $\overline{\lambda}(t)$ by a matrix inversion.

with the same number of initially infected nodes, no further immigrants, and
$\nu(t) = \beta e^{-\gamma t}$ [26]. This can be intuitively understood by considering that in
SIR the average, effective rate with which an infected individual generates new
infections after time t since it became infected equals β times the probability
that the node has not yet recovered, which is $e^{-\gamma t}$.

We remark that in [26] authors push this equivalence a bit further, by show-
ing that a SIR model with *finite* population N_0 is equivalent to a modulated
Hawkes process similar to (2), where $\mu(t) = 1 - N(t)/N_0$. In our model and its
application to COVID-19, we do not consider the impact of finite population
size, and assume an infinite population of susceptible individuals[3]. Therefore, we
do not need the 'correction factor' $1 - N(t)/N_0$, and instead use the modulating
function $\mu(t)$ to model the (process-independent) effect of mobility restrictions.
A similar effect due to mobility restrictions can be incorporated into the SIR
model, by applying factor $\mu(t)$ to the infection rate β.

Given the above connection between a (possibly modulated) Hawkes process
and the traditional SIR, one might ask what is the benefit of our approach with
respect to SIR-like models. In contrast to SIR, the Hawkes process allows us to
choose an arbitrary kernel $\nu(t)$, not necessarily exponential. With this freedom,
can we observe dynamics significantly different from those that can be obtained
by a properly chosen exponential shape? We answer this question in the positive
with the help of an illustrative scenario.

Consider an epidemic starting at time zero with $I_0 = 1000$ infected indi-
viduals.[4] We fix to $g = 10$ (days) the average generation time, which is the
mean temporal separation between a new infection belonging to generation i
and its parent in generation $i - 1$. Note that the above constraint implies that
$\int_0^\infty t \, \nu(t) \, \mathrm{d}t = g$.

---

[3]This assumption is largely acceptable at the beginning of an epidemic.

[4]Note that in our model the number of immigrants has a Poisson distribution with mean
$\int_0^\infty \sigma(t) \, \mathrm{d}t$. However to reduce the variance we have preferred to start simulations with the
same *deterministic* number of infected. Further, note that analytical results for the mean
trajectory of infected nodes are not affected by this choice.

We also normalize $\int_0^\infty \nu(t)\,\mathrm{d}t = 1$, since we can use $\mu(t)$ to scale the infection rate, in addition to considering time-varying effects due to mobility restriction. Note that in SIR we can only satisfy the above constraints by choosing the exponential kernel $\nu(t) = \frac{1}{g}e^{-\frac{t}{g}}$, $t > 0$. Instead, in our Hawkes model we have much more freedom.
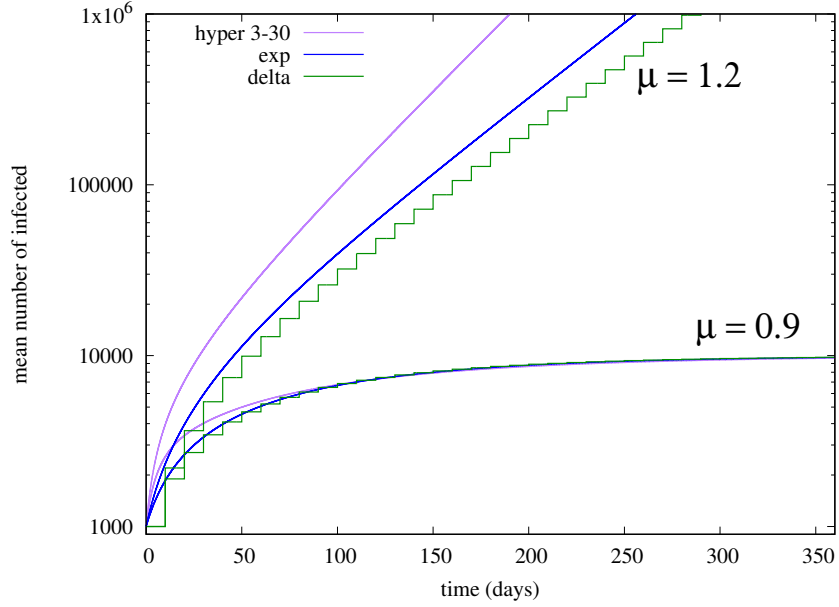

Figure 1: Evolution of mean number of infected for different kernel shapes, in the case of constant $\mu = 1.2$ (supercritical) or constant $\mu = 0.9$ (subcritical), with $I_0 = 1000$, $g = 10$.

First, we consider a scenario in which $\mu(t)$ is constant, equal to either 1.2 (supercritical case) or 0.9 (subcritical case). In Fig. 1 we show the temporal evolution of the mean number of infected $\overline{N}(t)$, for three kernel shapes that allows for an explicit solution of (4),(5) using Laplace transform (Appendix A). The *delta* shape corresponds to the kernel function $\overline{\nu}(t) = \delta(t - g)$, where $\delta(\cdot)$ is Dirac's delta function, for which

$$\overline{N}_{\mathrm{delta}}(t) = I_0 \frac{\mu^{\lfloor t/g \rfloor + 1} - 1}{\mu - 1} \tag{6}$$

The *exp* shape corresponds to the exponential kernel $\overline{\nu}(t) = \frac{1}{g}e^{-\frac{t}{g}}$ (SIR

model), for which

$$\overline{N}_{\exp}(t) = I_0 \left[1 + \frac{\mu}{\mu - 1} \left(e^{t(\mu-1)/g} - 1 \right) \right] \tag{7}$$

The *hyper* shape corresponds to the hyper-exponential kernel: $\overline{\nu}(t) = p_1 \alpha_1 e^{-\alpha_1 t} + p_2 \alpha_2 e^{-\alpha_2 t}$, where $0 \leq p_1 \leq 1$, $p_2 = 1 - p_1$, $p_1/\alpha_1 + p_2/\alpha_2 = g$, which also permits obtaining an explicit, though lengthy expression of $\overline{N}(t)$ that we omit here. Specifically, the 'hyper' curve on Fig. 1 corresponds to the case $1/\alpha_1 = 3$, $1/\alpha_2 = 30$.

We observe that, in the subcritical case ($\mu = 0.9$), the mean number of infected saturates to the same value, irrespective of the kernel shape; this can be explained by the fact that the final size of the epidemics is described by the same branching process for all kernel shapes (i.e., a branching process in which the offspring distribution is Poisson with mean 0.9). In the supercritical case ($\mu = 1.2$), instead, the mean number of infected grows exponentially as $\Theta(e^{\eta t})$ (as t grows large), where, interestingly, $\eta > 1$ depends on the particular shape (notice the log y axes on Fig. 1). In particular, the hyper-exponential kernel can produce arbitrarily large η (Appendix A). We conclude that, even when we fix the average generation time g, different kernels can produce largely different (in order sense) evolutions of $\overline{N}(t)$. Note that, by introducing compartments, SIR-like models can match higher-order moments of the generation time, but our results suggest that $\overline{N}(t)$ depends on *all* moments of it, i.e., on the precise shape of the kernel. Moreover, recall that some shapes are difficult to approximate by a phase-type approximation (e.g., the rectangular shape, or more in general, kernels with finite support).

The strong impact of the specific kernel shape becomes even more evident when we consider a time-varying $\mu(t)$, as in our modulated Hawkes process. As an example, consider the COVID-inspired scenario in which the modulating function $\mu(t)$ corresponds to the black curve in Fig. 2: during the first 30 days, $\mu(t)$ decreases linearly from 3 to 0.3; it stays constant at 0.3 for the next 60 days; and it goes back linearly to 3 during the next 30 days, after which it stays constant at 3.
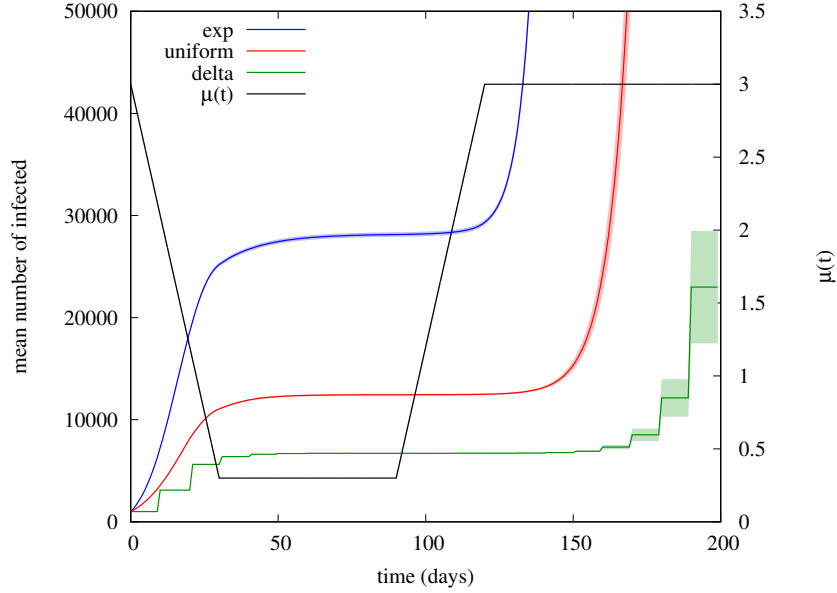
10

Figure 2: Evolution of mean number of infected (left y axes) in the COVID-like scenario, for different kernel shapes. Shaded areas denote 95%−level confidence intervals obtained by 100 simulation runs. The right y axes refers to modulating function $\mu(t)$ (black curve).

In Fig. 2 we show the mean number of infected estimated by simulation (averaging 100 independent runs), for the three kernel shapes *exp*, *delta*, and

205 *uniform*, where *uniform* corresponds to the kernel $\overline{\nu}(t) = \frac{1}{2g}$, $t \in (0, 2g)$, while the shapes *exp*, *delta* have been already introduced above. Shaded areas around each curve denote 95%−level confidence intervals.

We observe huge discrepancies among the trajectories of $\overline{N}(t)$ obtained under the three kernels. In particular, after the first 'wave' of 30 days, the *exp* kernel

210 produces about four times more infections than those produced by the *delta* kernel. This can be explained by the fact that $\mu(t)$ varies significantly on a time window (30 days) comparable to the average generation time (10 days).

It is also interesting to compare what happens on the second wave starting at day 90, after all 3 curves have settled down to an almost constant value:

215 now discrepancies are even more dramatic: although we observe a very fast resurgence of the epidemic in all cases, this happens with significant delays from

11

one curve to another. This is due to the fact that the number of individuals who are still infectious after the subcritical period (when $\mu < 1$) is largely different, especially considering that both the *uniform* and *delta* kernels have finite support (20 and 10 days, respectively) much smaller than the duration of the subcritical period, whereas the *exp* shape has infinite support: this implies that under the *uniform* and *delta* kernels the virus survives the subcritical period only through chains of infections belonging to successive generations, whereas under the *exp* shape in principle the epidemic can restart just thanks to the original immigrants at time 0, who are still weakly infectious when we re-enter the supercritical regime (around day 100). Actually, in our experiment, under the *delta* kernel the epidemic died out in 68 out of 100 simulation runs, which explains the large confidence intervals obtained in this case at end of the observation window. Under the *uniform* kernel, the epidemic died only in 3 out of 100 runs, while it always survived under the *exp* kernel.

We conclude that, even while fixing the mean generation time, the precise shape of the kernel function can play an important role in predicting the process dynamics and the impact of countermeasures, especially when the time-scale of control is comparable to the time-scale of an individual contagion. One might obtain a good fitting with measured data also by using an exponential shape, and a properly chosen modulating function $\mu(t)$, but this is undesirable, since the required $\mu(t)$ would no longer reflect the actual evolution of mobility and interpersonal contact restrictions. In the case of COVID-19, several researchers have actually attempted to incorporate into analytical models detailed information about people mobility, using for example data provided by cellular network operators or smartphone apps [27, 28].

In Appendix B we elaborate more on this point by examining also the SEIR model, which, with respect to the classic SIR, provides an additional compartment to better describe the dynamics of an individual infection.

4. Moment generating function

Our modulated Hawkes process is stochastic in nature, hence it is important to characterize how realizations of the process are concentrated around the mean trajectory derived in Sec. 2. This characterization is instrumental, for example, in designing simulation campaigns with proper number of runs. Moreover, note that it is entirely possible that the epidemic gets extinct at its early stages, or in between two successive waves, as we have seen in the scenario in Fig. 2. Actually, an epidemic could die out even when starting in the supercritical regime (consider the case of a single immigrant at time t, who does not generate any offspring with probability $e^{-R(t)}$), something that is not captured by deterministic mean-field approaches. Therefore, it is interesting to understand the variability of the process at any time.

Under mild assumptions an expression for the moment generating function of the number of points in $[0, t)$ can be given, and an iterative procedure can be applied to compute the moment of any order n in terms of moments of smaller order, though with increasing combinatorial complexity.

In this section we limit ourselves to reporting the main results on this moments' characterization, without their mathematical proofs, to keep the paper focused on the application to COVID-19 and its control measures.

Hereon, we shall assume

$$K_1 := \sup_{(t,m)\in(0,\infty)\times M} \nu(t, m) \in (0, \infty), \quad K_2 := \sup_{t\in(0,\infty)} \mu(t) \in (0, \infty). \quad (8)$$

Also, we fix a horizon $\tau \in (0, \infty)$, and, for $t \in (0, \tau)$, we denote with $S_{t,\tau}$ the number of points, up to time τ, in the cluster generated by an immigrant at t (including the immigrant). We denote with $|\cdot|$ the modulus of a complex number.

We are interested in $N(\tau)$, i.e., the total number of points generated up to time τ, irrespective of their mark.

Theorem 4.1 (Moment generating function of $N(\tau)$). *Assume* (1) *and* (8).

Then there exists $\theta_c > 0$ such that, for any $z \in \Theta_c$,

$$\Theta_c := \{z \in \mathbb{C} : \ \mathrm{Re}\, z < \theta_c\},$$

we have

$$\mathbb{E}[\mathrm{e}^{zN(\tau)}] = \exp\left(\int_0^\tau (G(t, z) - 1)\, \sigma(t)\mathrm{d}t\right) \tag{9}$$

and

$$\sup_{z \in \Theta_c} |\mathbb{E}[\mathrm{e}^{zN(\tau)}]| < \infty. \tag{10}$$

Here

$$G(t, z) := \mathbb{E}[\mathrm{e}^{zS_{t,\tau}}], \tag{11}$$

is the solution of the following functional equation.

$$G(t, z) = \mathrm{e}^z \mathbb{E}\left[\mathrm{e}^{\int_0^\tau (G(v,z)-1)\mu(v)\nu(v-t, M_1)\, \mathrm{d}v}\right], \quad (t, z) \in (0, \tau) \times \Theta_c. \tag{12}$$

From the moment generating function we can obtain an expression for the first and second moment of $N(\tau)$ (the first moment can also be obtained directly from the average stochastic intensity, as we have done in Sec. 2.).

Theorem 4.2 (The first two moments of $N(\tau)$). *Assume (1) and (8). Then*

$$\mathbb{E}[N(\tau)] = \overline{N}(\tau) = \int_0^\tau \overline{\lambda}(t)\, \mathrm{d}t = \int_0^\tau E_1(t)\sigma(t)\, \mathrm{d}t \tag{13}$$

and

$$\mathbb{E}[N(\tau)^2] = \int_0^\tau E_2(t)\sigma(t)\, \mathrm{d}t + \left(\int_0^\tau E_1(t)\sigma(t)\, \mathrm{d}t\right)^2, \tag{14}$$

with

$$E_2(t) = G''(t, 0) = \mathbb{E}[S_{t,\tau}^2] = 1 + \int_t^\tau E_2(v)\mu(v)\overline{\nu}(v - t)\, \mathrm{d}v +$$

$$+ 2\int_t^\tau E_1(v)\mu(v)\overline{\nu}(v - t)\, \mathrm{d}v + \left(\int_t^\tau E_1(v)\mu(v)\overline{\nu}(v - t)\mathrm{d}v\right)^2 \tag{15}$$

$$E_1(t) = G'(t, 0) = \mathbb{E}[S_{t,\tau}] = 1 + \int_t^\tau \overline{\lambda^{(t)}}(v)\, \mathrm{d}v \tag{16}$$

and

$$\overline{\lambda^{(t)}}(v) = \mu(v)\overline{\nu}(v - t) + \mu(v)\int_t^v \overline{\nu}(v - u)\overline{\lambda^{(t)}}(u)\, \mathrm{d}u. \tag{17}$$

14

Note that (15) and (17) are second-type inhomogeneous Volterra equations.

²⁷⁵ In the particular case in which $\mu()$ is constant, solutions for (15) and (17) can be found by applying a standard Laplace transform methodology.

5. COVID-19 Model

Now we describe how we applied the modulated Hawkes process introduced before to model the propagation dynamics of COVID-19. The proposed model

²⁸⁰ could actually be used to represent the dynamics of other similar viruses as well.

First, we take advantage of the fact that we do not need to consider a unique kernel function for all infected. Indeed, the presence of marks allows us to introduce different classes of infectious individuals with specific kernel functions. Specifically, we have considered three classes of infectious: *symptomatic*, *asymp-*

²⁸⁵ *tomatic* and *superspreader*, denoted by symbols $\{s, a, h\}$. We assume that, when a person gets infected, it is assigned a random class $C \in \{s, a, h\}$ with probabilities p_s, p_a, p_h, respectively, $p_s + p_a + p_h = 1$, $0 \leq p_s \leq 1$, $0 \leq p_a \leq 1$, $0 \leq p_u \leq 1$.

As the name suggests, *symptomatic* people are those who will develop evi-

²⁹⁰ dent symptoms of infection, and we assume that because of that they will be effectively quarantined at home or hospitalized at the onset of symptoms. On the contrary, the *asymptomatic* mark is given to individuals who will not develop strong enough symptoms to be quarantined. Therefore, they will be able to infect other people for the entire duration of the disease, though at low in-

²⁹⁵ fection rate (unless they get scrutinized by mass testing, as explained later). At last, *superspreaders* are individuals who exert a high infection rate but do not get quarantined due to several possible reasons (unless they get scrutinized by mass testing). This class also includes people with mild symptoms, who become highly contagious because of their mobility pattern (e.g., participation to 'su-

³⁰⁰ perspreading events'). Though the above classification of infectious individuals is a simplified one, a properly chosen mix of the three considered classes can represent a wide range of different scenarios.

15

Irrespective of their class, we will assume that all infectious people go through the following sequence of stages: first, there is a random incubation time, denoted by r.v. I, with given cdf $F_I()$. During this time we assume the all infected exert a low infection rate λ_{low}. Then, there is a crucial pre-symptomatic period, during which infected in classes $\{s, h\}$ already exert a high infection rate λ_{high}, while infected in class a still exert low infection rate λ_{low}. For simplicity, we have assumed the presymptomatic phase to have constant duration w.

The following evolution of the infection rate of an individual depends on the class: since we assume that *symptomatic* people get effectively quarantined, they no longer infect other individuals after the onset of symptoms. We model this fact introducing a *quarantined* class of people (denoted by q), and deterministically moving all infected in class s to class q after time $I + w$.

People in classes $\{a, h\}$ continue to be infectious during a disease period of random duration D, with given cdf $F_D()$. The difference between these two classes is that infectious in class a (h) exert, during the disease period, infection rate λ_{low} (λ_{high}), respectively. At last, we assume that people in classes $\{a, h\}$ enter a residual period of random duration E, with cdf $F_E()$, during which all of them exert infection rate λ_{low}. We introduced this additional phase because some people who recovered from COVID-19 where found to be still contagious several days (even weeks) after the end of the disease period. Note that durations I, D, E are assumed to be independent, and that the complete mark associated to an infected is the 4-tuple $M = (C, I, D, E)$.

An illustration of the three class-dependent kernels $\nu(t, s), \nu(t, a), \nu(t, h)$, conditioned on the durations (I, D, E), is reported in Fig. 3.

Remark 5.1. *We emphasize that our model of COVID-19 is targeted at predicting the process of new infections, rather than the current number of people hosting the virus in various conditions. In particular, we do not explicitly describe the dynamics of symptomatic but quarantined people and their exit process (i.e., recovery or, in the worst case, death), since such dynamics have no effect on the spreading process (under the assumption of perfect quarantine). How-*
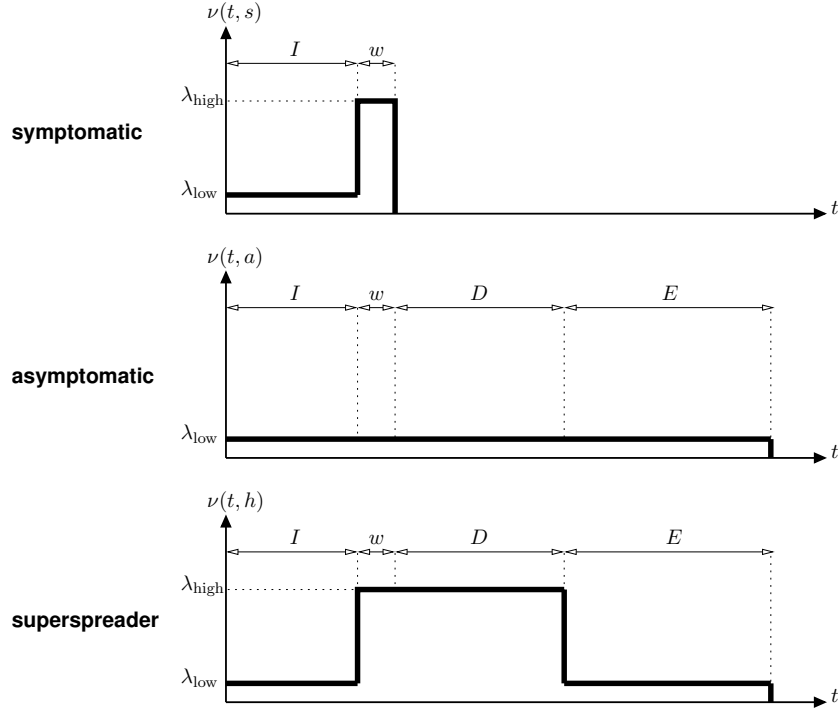
16

Figure 3: Kernel functions for classes s, a, h (from top to bottom), for given durations I, D, E of stages.

ever, if desired, one could describe through appropriate probabilities and time distributions how quarantined people split between those isolated at home and those who get hospitalized, the fraction going to intensive care, and those who unfortunately die.

Remark 5.2. *The use of 'classes' and 'stages' in our model is similar to the classical approach of introducing compartments in models stemming from the basic SIR of Kermack and McKendrick. The fundamental difference is that in our marked Hawkes model we can consider arbitrary distributions for the time spent in stages, and account for the non-homogeneous intensity of offsprings generated by an infected during a stage. Moreover, note that an Hawkes process has a rich (non Markovian) stochastic structure, whereas compartmental models are usually analyzed by ordinary differential equations.*

17

Parameter	symbol	COVID-19 fitted value
incubation period	I	tri([2,12], mean 6)
pre-symptoms period	w	2
disease period	D	unif([2,12])
residual period	E	exp(10)
low infection rate	λ_{low}	0.05
high infection rate	λ_{high}	1
symptomatic probability	p_s	0.06
asymptomatic probability	p_a	0.91
super-spreader probability	p_h	0.03

Table 1: Virus-specific parameters.

The parameters introduced so far, summarized in Table 1, are related to specific characteristics of the virus. We now model properties of the specific environment where the virus spreads, taking into account the impact of countermeasures. First, we need to specify the immigration process $\sigma(t)$. To keep the model as simple as possible, we have assumed that the system starts at a given time with I_0 new infections, i.e., immigrants arrive as a single burst concentrated at one specific instant.

The impact of countermeasures is taken into account in the model in two different ways. First, modulating function $\mu(t)$ can be used to model the instantaneous reduction of the infection rate at time t due to the current mobility restrictions, and, more in general, changes in the environment which affect the ability of the virus to propagate in the susceptible population (such as seasonal effects). Typically, $\mu(t)$ is a decreasing function in the initial part of the epidemics, in response to new regulations introduced by the government, while it goes up again when mobility restrictions are progressively released.

Second, we assume that any infected not already found to be positive is tested (e.g., by means of massive swab campaigns) at individual, instantaneous rate $\rho(t)$, which reflects both the amount of resources employed by the health

service to discover the infected population, and the effectiveness of tracking. Recall that, when an infected is found positive, we assume it transits to the quarantined state q and stops infecting other people.
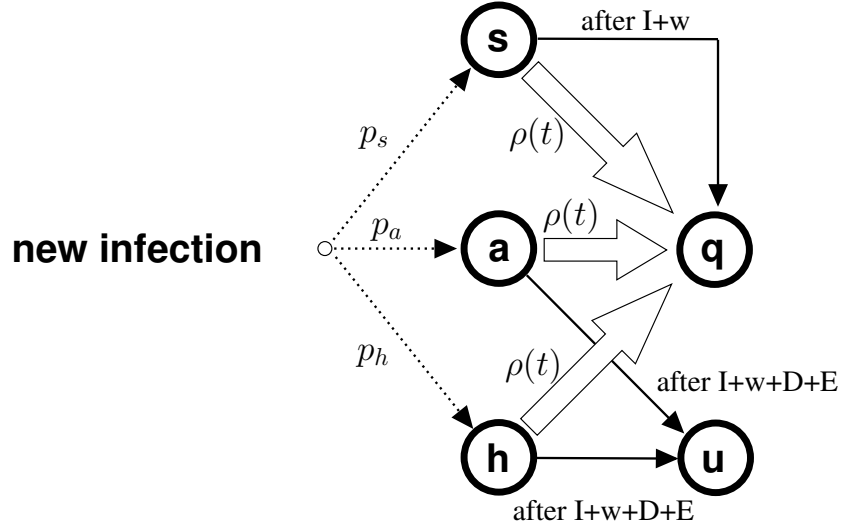

Figure 4: State transitions of an infected individual.

Fig. 4 shows the resulting transitions that can occur for the different classes. Note that class q collects all cases known to the health authorities at a given time t, and thus coincides with the set of detected cases. Infected in classes s, a, h are still unknown to the health service (but they are detectable). When they stop to be positive, people in classes a, h transit to a class u (undetected), which collects all infected who remain unknown to the health service.

Environment-related parameters are summarized in Table 2.

Remark 5.3. *We emphasize that the model described so far does not explicitly model spatial effects and sub-populations. As such, it is more suitable to describe a homogeneous scenario, where its environmental parameters (including modulating functions $\mu(t)$ and detection rate $\rho(t)$) can be reasonably assumed to apply to all individuals of the population irrespective of their spatial location. The natural candidate of such scenario is a single nation or just a sub-region of it. By so doing, we can assume that common national regulations are ap-*

19

Parameter	symbol	fitted value for first wave in Italy
initial day	$-\Delta t$	-20
initial number of infected	I_0	370
modulating function	$\mu(t)$	$T_a = -3$, $\mu_a = 3.71$
		$T_b = 30$, $\mu_b = 0.31$, (see Fig. 5)
detection rate	$\rho(t)$	$\rho(t) = 0.000115\, t$, (see Fig. 5)

Table 2: Environment-specific parameters.

380 *plied, as well as common health-care practices. However, our approach based on Hawkes processes could be extended to incorporate spatial effects, by considering spatio-temporal kernel functions $\nu(\boldsymbol{x}, t)$, where $\boldsymbol{x}$ is a spatial vector originated at the point at which a new infection occurs. Another possibility would be to consider a multivariate temporal Hawkes process, where each component rep-*
385 *resents a homogeneous region, and the different regional processes can interact with each other.*

5.1. Computation of the real-time reproduction number $R(t)$

From our model, it is possible to compute in a native way the average number of infections caused by an individual who gets infected at time t, i.e., the real-time reproduction number $R(t)$. To compute $R(t)$, we condition on the duration x of the incubation time, on the duration y of the disease time, on the duration z of the residual time, and on the class assigned to the node getting infected at time t (note that they are all independent of each other):

$$R(t) = \int_x \int_y \int_z \left(\lambda_{\text{low}} \int_0^x \mu(t+\tau) u(t,\tau)\, \mathrm{d}\tau + p_a \lambda_{\text{low}} \int_x^{x+w+y+z} \mu(t+\tau) u(t,\tau)\, \mathrm{d}\tau + \right.$$

$$(p_s + p_h)\lambda_{\text{high}} \int_x^{x+w} \mu(t+\tau) u(t,\tau)\, \mathrm{d}\tau + p_h \lambda_{\text{high}} \int_{x+w}^{x+w+y} \mu(t+\tau) u(t,\tau)\, \mathrm{d}\tau +$$

$$\left. p_h \lambda_{\text{low}} \int_{x+w+y}^{x+w+y+z} \mu(t+\tau) u(t,\tau)\, \mathrm{d}\tau \right) \mathrm{d}F_E(z)\, \mathrm{d}F_D(y)\, \mathrm{d}F_I(x) \quad (18)$$

20

where

$$u(t,\tau) = e^{-\int_t^{t+\tau} \rho(s)\, ds}$$

is the probability that a node which gets infected at time t is still undetected at time $t + \tau$.

6. Model fitting for the first wave of COVID-19 in Italy

We fit the model to real data related to the spread of COVID-19 in Italy, publicly available on GitHub [29]. Italy was the country where the epidemics first spread outside of China into Europe, causing about 34600 deaths at the end of June 2020 during the first wave.

Our main goal was to match the evolution of the number of detected cases, represented in the model by individuals in class q. The actual count is provided by the Italian government on a daily basis since February 24th 2020. We take this date as our reference day zero. However, it is largely believed that the epidemics started well before the end of February. Indeed, it became soon clear that detected cases were just the top of a much bigger iceberg, as the prevalence of asymptomatic infection was initially largely unknown, which significantly complicated the first modeling efforts to forecast the epidemic evolution. During June-July 2020, a blood-test campaign (aimed at detecting IgG antibodies) was conducted on a representative population of 64660 people to understand the actual diffusion of the first wave of COVID-19 in Italy [30]. As a main result, it has been estimated that 1 482 000 people have been infected. This figure provides a fundamental hint to properly fit our model, and indeed while exploring the parameter space we decided to impose that the total number of predicted cases at the end of June (day 120) is roughly 1 500 000.

For the durations I,w,D,E of the different stages of an infection, we have tried to follow estimates in the medical literature. In particular, the duration of the incubation period is believed to range between 2 and 12 days, with a sort of bell shape around about 5 days [31, 32, 33], which we have approximated, for simplicity, by a (asymmetric) triangular distribution with support $[2, 12]$ and

21

mean 6. Moreover, we have fixed the duration of the pre-symptomatic phase
to 2 days. For the duration of the disease period we have taken a uniform
distribution on $[2, 12]$, while the residual time is modeled by an exponential
distribution with mean 10 days [34].

The other virus-related parameters have been set as reported in the third
column of Table 1. Note that, since we further apply the external modulating
function $\mu(t)$, we could arbitrarily normalize to 1 the value of λ_{high}, while we
set $\lambda_{\mathrm{low}} = 0.05$.

For what concerns environment-related parameters (see Table 2), a first
problem was to choose a proper initial day $-\Delta t$ (recall that day zero is the
first day of the trace) at which to start the process with I_0 initially infected
individuals. While different pairs $(\Delta t, I_0)$ are essentially equivalent, we decided
not to start the process with too few cases and too much in advance with respect
to day 0, to limit the variance of a single simulation run. We ended up setting
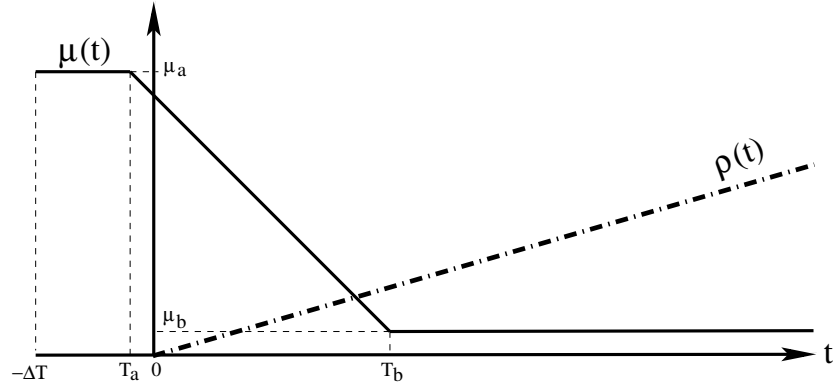$\Delta t = 20$, while $I_0 = 370$ was selected as explained later.

Figure 5: Chosen profiles and parameters of functions $\mu(t)$ and $\rho(t)$ for the first wave of
COVID-19 in Italy.

Mobility restrictions in Italy were progressively enforced by national laws
starting a few days before day 0, first limited to red zones in Lombardy, and
soon extended to the entire country through a series of increasingly restrictive
regulations, introduced over the next 30 days. Instead of trying the capture the

22

step-wise nature of such restrictions, we assume $\mu(t)$ to take the simpler profile

depicted in Figure 5, i.e., a high initial value μ_a before time T_a, a low final value μ_b after time T_b, and a linear segment connecting point (T_a, μ_a) to point (T_b, μ_b). We decided to set $T_a = -3$ and $T_b = 30$ to reflect the time window in which mobility restriction were introduced.

In Fig. 5 we also show our choice for the profile of detection rate $\rho(t)$, i.e., a linear increase starting from day 0, with coefficient α, $\rho(t) = \max\{0, \alpha t\}$. This profile is justified by the fact that the first wave caught Italy totally unprepared ($\rho = 0$ before day zero), while massive swabs were only gradually deployed over time after day zero.

The critical parameters $I_0, \mu_a, \mu_b, \alpha$ were fitted by a minimum mean square error (MMSE) estimation technique based on the curve of detected cases in the time window $[0 - 120]$ days, after all other parameters were manually selected as detailed above.
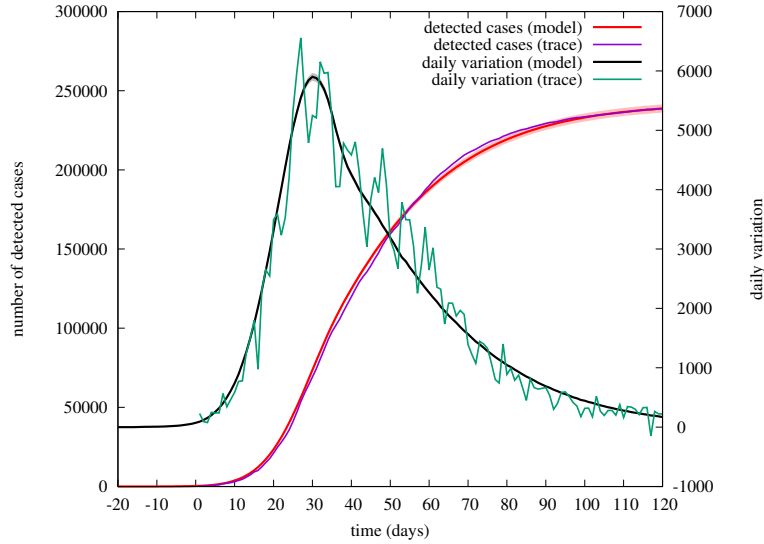

Figure 6: Evolution of the number of detected cases according to model and real data. Cumulative number (left y axes) and its daily variation (right y axes).

Fig. 6 shows the final outcome of our fitting, comparing the evolution of the number of detected cases according to model and real data. We show both
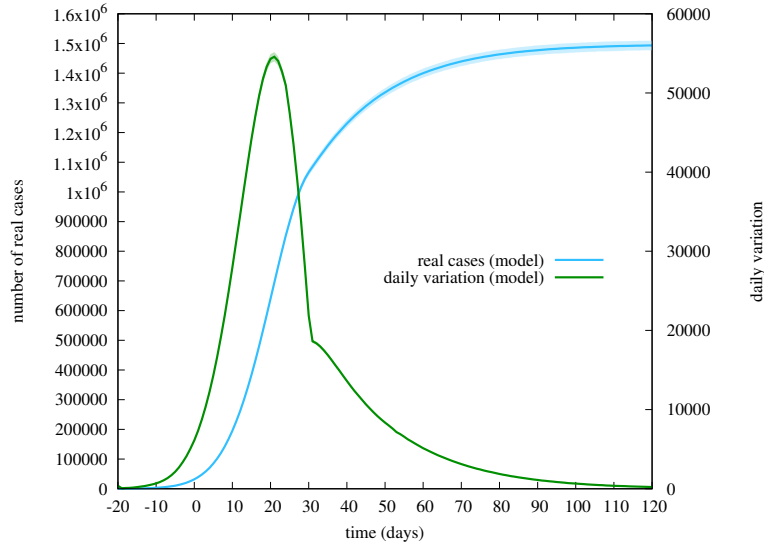
23

Figure 7: Evolution of the actual number of cases according to model only. Cumulative number (left y axes) and its daily variation (right y axes).

the cumulative number (left y axes) and its daily increment (right y axes). Analytical predictions for the mean trajectory of detected cases were obtained by averaging 100 simulation runs. The shaded region around analytical curves (barely visible) shows 95%-level confidence intervals computed for each of the 120 days.

We emphasize that a similar good match could be possibly obtained by other sets of parameters. Our purpose here was not to compute the best possible fit in the entire parameter space (which would be nearly impossible), but to show that the model is rich enough to capture the behavior observed on the real trace after a reasonable choice of most of its parameters, driven by their physical meaning.

Fig. 7 shows instead the evolution of the real number of cases (both the cumulative number and its daily variation) according to the model only, in the absence of data. Note however that we have constrained ourselves to obtain a total number of about 1 500 000 cases on day 120, as suggested by the serological test [30].

24

Interestingly, by looking at the values of μ_a and μ_b computed by our MMSE, it appears that the national lockdown was able to reduce the spreading ability of the virus within the Italian population by a factor of about 12 (from 3.71 to 0.31). We will see later on in Fig. 12 that our fitting of $\mu(t)$ for the first wave is consistent with mobility trends estimated from the usage of the Apple maps application [28].
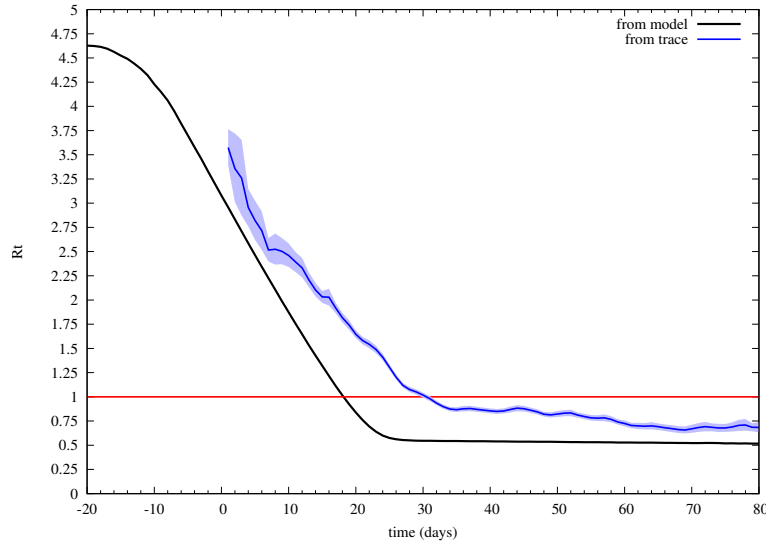

Figure 8: Real-time reproduction number computed by the model, compared to its estimation based on the trace of detected case, according to the Wallinga-Teunis method (with 95% confidence interval denoted as shared region).

In Fig. 8 we show the real-time reproduction number computed by (18). We also applied the classic method of Wallinga-Teunis [35], implemented as in the R0 package [36], to estimate $R(t)$ from the trace of detected cases. To apply their method, we used a generation time obtained from a Gamma distribution with mean 6.6 (shape 1.87, scale 0.28), which has been proposed for the first wave of COVID-19 in Italy [37]. Interestingly, though both estimates of $R(t)$ exhibit qualitatively the same behavior, the model-based value of $R(t)$, which considers also undetected cases, tends to be smaller.

25

6.1. What-if scenarios

Having fitted the model to the available trace, we proceed to exploit the model to examine interesting what-if scenarios. First, we investigate what would have happened (according to the fitted model) if lockdown restrictions were shifted in time by an amount of days δ. This means that we keep all parame-ters the same, except that we translate horizontally in time the profile of $\mu(t)$ depicted in Fig. 5. In Figure 9 we show the total number of cases that would have occurred for values of $\delta \in \{-7, -3, 0, 3, 7\}$.
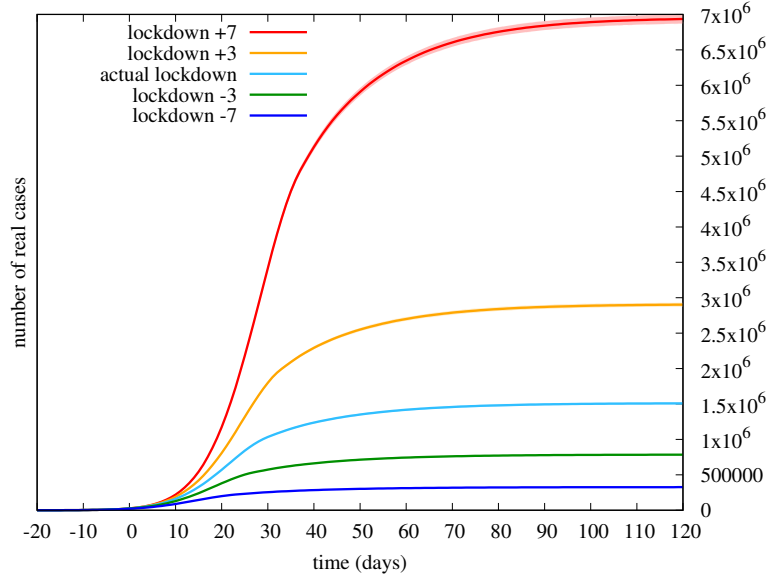

Figure 9: What-if scenario: total number of cases if restrictions were shifted in time by δ days.

We observe that a shift of just 3 days corresponds to a factor of roughly 2 in the number of cases. This translates, dramatically, into an equivalent impact on the number of deaths, if we assume that the mortality rate would have stayed the same[5] (i.e., $34600/1500000 \sim 2.3\%$). In other words, a postponement (anticipation) of lockdown restrictions by just 3 days would have caused twice

---

[5]This is somehow optimistic, since mortality also depends on the saturation level of inten-sive therapy facilities.

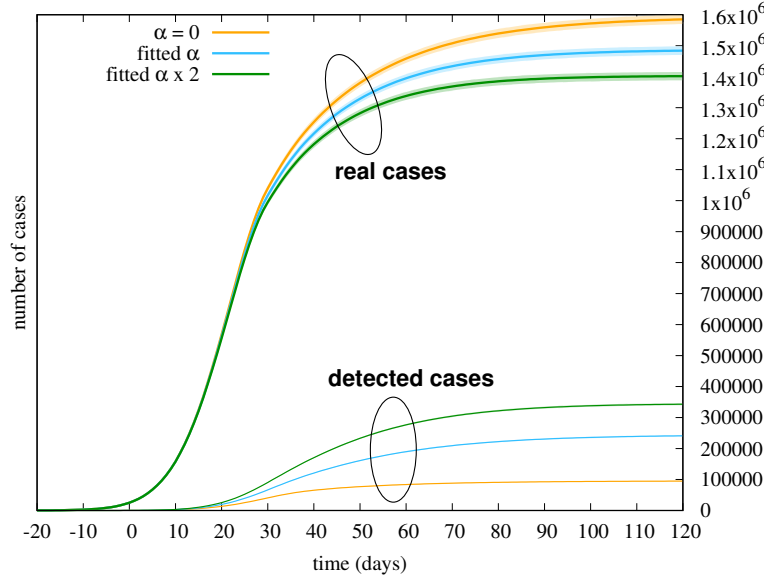(half) the number of deaths, which is a rather impressive result.

Figure 10: What-if scenario: impact of detection rate $\rho(t) = \alpha t$ on the real and detected number of cases, varying α.

In Figure 10 we investigate instead the impact of detection rate $\rho(t)$, by
changing its slope α (recall Fig. 5). We report both the number of real cases
and the number of detected cases predicted by the model, when all other fitted
parameters are kept the same. We consider what would have occurred with
$\alpha = 0$ (which means that infectious people are never tested), and by doubling
the intensity of the detection rate (a tracking system twice more efficient). As
expected, with $\alpha = 0$ only symptomatic cases ($p_s = 6\%$) are eventually detected.
This time the effect on the final number of cases (or deaths) is not as dramatic as
in the previous what-if scenario. This suggests that the impact of mass testing
in Italy during the first wave was marginal, and doubling the efforts would not
have produced significant changes in the final outcome.

7. Model fitting for the second wave of COVID-19 in Italy

The second wave of COVID-19 hit Italy in late summer 2020, as in many other European countries, mainly as en effect of relaxed mobility in July/August and possibly other seasonal effects. It is interesting to compare the second wave with the first wave, by looking at the daily increments of detected cases and deaths, see Fig. 11.
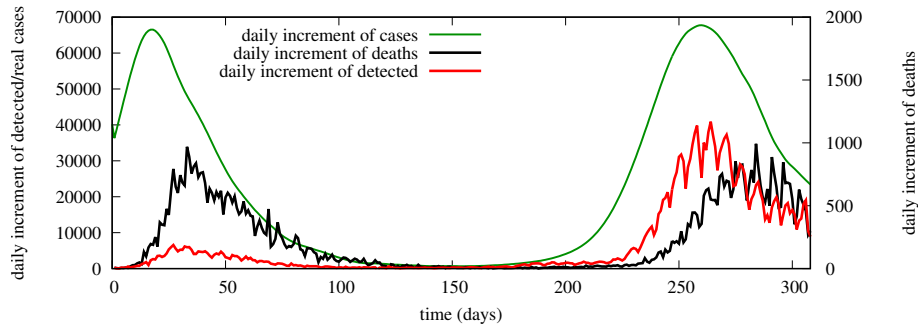

Figure 11: Daily increment of the number of deaths (black curve, right y-axes), daily increment of the number of detected (red curve, left y axes), and estimated daily increment of real cases projected back from the curve of deaths (green curve, left y-axes).

We observe that the number of daily deaths is similar between the two waves. The daily increment of detected cases, instead, is very different (around 5000 at the peak of the first wave, around 35000 at the peak of the second wave, a 7-fold increase). This can be explained by the much larger capacity of the health service to perform swabs and track down the infected, built on the experience gained from the first wave. It also suggests that, differently from the first wave, the impact of $\rho(t)$ (the individual rate at which an infectious is detected) is expected to be much more important during the second wave than in the first wave, requiring a careful treatment of it in the model.

We have indeed tried to fit our model to the second wave in Italy, keeping all parameters related to the virus (previously fitted for the first wave) unchanged (Table 1), and adapting only environment-specific parameters (Table 2). A major difficulty that we had to face was the unknown (at the time of writing)

28

actual diffusion of the virus in the population during the second wave. Recall that, for the first wave, we exploited a blood-test campaign to get a reference for the total number of real cases at the end of the first wave. For the second wave we employed instead a different approach based on a projection back in the past of the increment of deaths. A similar idea has been adopted in [38] to estimate the time-varying reproduction number in different European country at the onset of the first wave.

Specifically, we got from [39] the indication of the median (11 days) and IQR (6-18 days) of the amount of time from symptoms onset to death during Oct-Dec 2020, that we fitted by a Gamma distribution (shape 1.65, scale 8.45). By convolving such Gamma distribution with the distribution of incubation time, and the pre-symptoms period, we obtained a distribution of the total time from infection to death, that we used to estimate the time in the past at which each dead person was initially infected. By amplifying the number of infections leading to death by the inverse of the mortality rate we eventually obtained an estimate of the daily increment of real cases, as reported in Fig. 11 (green curve, left y-axes).

We chose August 1st (day 160 on Fig. 11) as starting date of the new infection process producing the second wave in Italy. This time, instead of manually searching for suitable profiles of $\mu(t)$ and $\rho(t)$ generating the expected curves of real and detected cases, we adopted a novel "reverse-engineering" approach: we took the daily increments of real and detected cases as input to the model, and computed the functions $\mu(t)$ and $\rho(t)$ that would exactly produce in the model the given numbers of real and detected cases, on each day[6].

In Fig. 12 we show the obtained 'reversed' $\mu(t)$ (blue curve), starting from day 0 (August 1st) of the time reference adopted for the second wave. We also report the average mobility measured in Italy by the Apple maps application

---

[6]Discretized values of functions $\mu(t)$ and $\rho(t)$ are uniquely determined in the model, once we constrain ourselves to produce a given number of real and detected cases at each time instant.
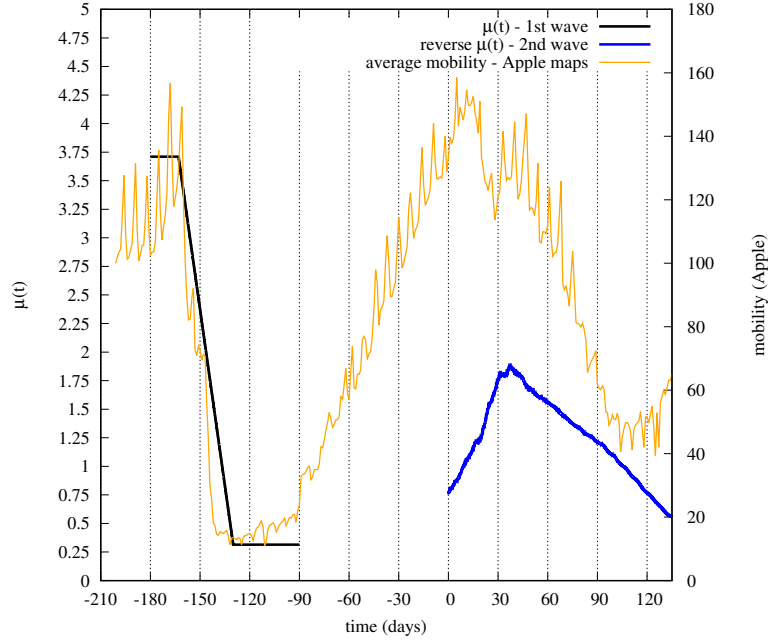
Figure 12: Modulating functions $\mu(t)$ for the first wave (black, fitted) and second wave (blue, reversed), and average mobility according to Apple maps application.

[28], where we have given equal weight (1/3) to driving, transit and walking mobility. We observe that the 'reversed' $\mu(t)$ qualitatively follows the same behavior of mobility measured on the maps application, with a gradual increase during the month of August followed by a gradual decrease as people (and the government) started to react to the incipient second wave.

For completeness, we have also reported on Fig. 12 the fitted $\mu(t)$ for the first wave (black curve). We observe that, during the first wave, the quick introduction of hard lockdown caused an abrupt decay of both measured mobility and fitted $\mu(t)$, characterized by a bigger reduction in a shorter time. The second wave, instead, was characterized by a smoother transition, due to the different choice of applying just partial lockdowns and progressive restrictions more diluted over time[7].

---

[7]The fact that, during the second wave, mobility values similar to those of the first wave

30

In Fig. 13 we show instead the 'reversed' function $\rho(t)$, focusing on the second wave. We also report on the same plot the daily increments of real and detected cases, which allow us to better understand the obtained profile of $\rho(t)$, highlighting an interesting phenomenon occurred around day 30. Indeed, we observe that, during the first month, the epidemic was closely tracked by the national health system, but at some point, around day 30, the curve of detected cases stops increasing, and stays roughly constant during the entire second month, lagging more and more behind the otherwise exploding curve of real cases (time window 30-60). As consequence, function $\rho(t)$, which describes the effectiveness of individual tracking, falls down to a minimum reached at around day 60. This behavior can be interpreted as an effect of the saturation of the capacity to perform swabs, resulting in a progressive collapse of the tracking system, as actually experienced by many people during those days.

Our analysis shows that, in contrast to what might be believed by just looking at the curve of detected cases, September (days 30-60) was, perhaps, the most critical period for the outbreak of the second wave of COVID-19 in Italy. During this period, the detection capacity of the national health system was saturated, and could not keep the pace with the rapid growth of real cases, giving instead the illusion of maintaining the epidemic under control. Our reverse-engineering approach can thus shed some light on what actually happened at the onset of the second wave, and *quantitatively* assess the collapse of the tracking system.

8. Conclusions

We have proposed a time-modulated version of the Hawkes process to describe the temporal evolution of an epidemic within an infinite population of susceptible individuals. Our approach allows us to take into account precise distributions for the time spent in different stages of the infection, which is

do not translate into equally similar values of $\mu(t)$ can be attributed to increased awareness of people during the second wave.
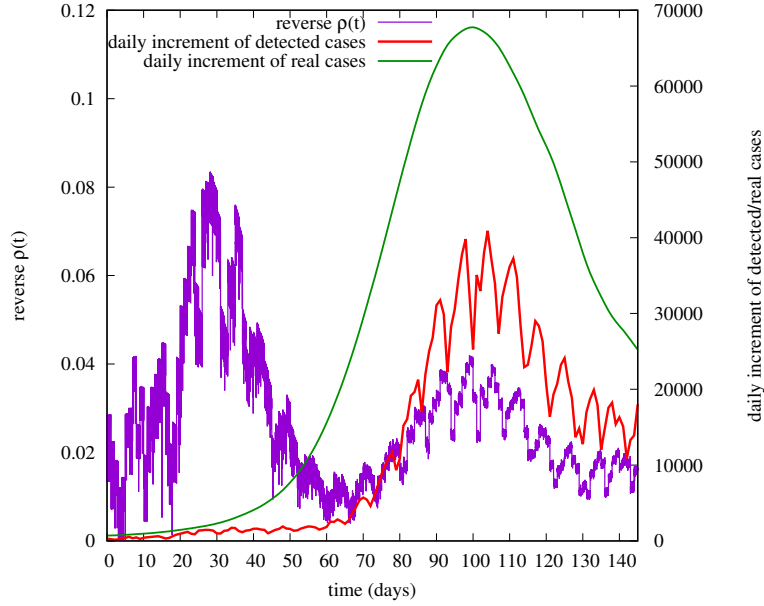
Figure 13: Reverse detection rate $\rho(t)$ for the second wave (left y-axes), and daily increase of real and detected cases (right y-axes).

of paramount importance when the intensity of countermeasures (mobility restrictions, testing and tracing) varies significantly on time-scales comparable to that of an individual infection. We have applied the model to the spread of COVID-19 in Italy, either by a direct fit of its parameter (first wave), or by a novel reverse fit (second wave) which allows us, in retrospect, to understand from data the time-varying effectiveness of applied countermeasures. Future work will extend the model to overcome some of its current limitations, like the impact of spatial effects and other sources of heterogeneity in the population, such as age groups. We think the proposed approach is promising and could be usefully applied to explain the epidemic progress and forecast/assess the impact of control/mitigation measures.

32

Appendix A. Explicit solution of $\overline{\lambda}(t)$ for constant $\mu(t) = \mu$

When $\mu(\cdot) \equiv \mu$ is constant, denoting with $*$ the convolution product, we can rewrite equation (4) as

$$\overline{\lambda}(t) = \sigma(t) + \mu \cdot (\overline{\nu} * \overline{\lambda})(t), \quad t > 0,$$

which can be easily solved in the transformed domain. For a non-negative function $f : \mathbb{R}_+ \to \mathbb{R}_+$, we denote by

$$\widehat{f}(s) := \int_{\mathbb{R}_+} e^{-st} f(t) \, dt, \quad s \in \mathbb{C}$$

the Laplace transform of f. Then we have:

$$\widehat{\overline{\lambda}}(s) = \frac{\widehat{\sigma}(s)}{1 - \mu\widehat{\overline{\nu}}(s)} \qquad \text{for } \mathrm{Re}(s) > \mathrm{Re}(z_{\max}),$$

with $z_{\max}$ equal to the zero of $1 - \mu\widehat{\overline{\nu}}(s)$ with largest real part.

In addition, formally, as long as $\mu < 1$ and σ is bounded, we can write

$$\overline{\lambda}(t) = \sigma(t) + \sigma(t) * \sum_{i=1}^{\infty} \mu^i \overline{\nu}^{*i}(t)$$

where $\overline{\nu}^{*i}(t)$ is the i-th fold convolution of $\overline{v}(t)$.

An analytical expression of $\overline{\lambda}(t)$ can be obtained when $\sigma(s)$ and $\overline{\nu}(s)$ are both rational. Table A.3 reports the dominant[8] term of $\overline{\lambda}(t)$ (and also of $\overline{N}(t)$) for the case in which $\sigma(t) = \beta \exp(-\beta t)$, and $\overline{\nu}(t)$ takes different shapes satisfying:

$$\int_0^{\infty} \overline{\nu}(t) \, dt = 1 \quad ; \quad \int_0^{\infty} t \, \overline{\nu}(t) \, dt = \frac{1}{\alpha}$$

Besides the simple deterministic (*delta*) and exponential (*exp*) shapes, we consider the Erlang-2 (*erl-2*) and two variants of hyper-exponential, whose general form is $\overline{\nu}(t) = p_1\alpha_1 e^{-\alpha_1 t} + p_2\alpha_2 e^{-\alpha_2 t}$. To reduce the degrees of freedom of the general hyper-exponential, we have assumed a particular relationship between p_1/p_2 and α_1/α_2, which allows us to introduce a single parameter z.

---

[8]We recall that a non negative function $f(t)$ is said to be $\Theta(1)$, iff there exist two constants $0 < c \leq C < \infty$ such that $c \leq f(t) \leq C$, for sufficiently large t.

33

shape	$\overline{\nu}(t)$	$\overline{\lambda}(t)$
delta	$\delta(t - \frac{1}{\alpha})$	$\Theta(1)\,\mathrm{e}^{\alpha \log(\mu)t}$
erl-2	$(2\alpha)^2 t\,\mathrm{e}^{-2\alpha t}$	$\Theta(1)\,\mathrm{e}^{2\alpha(\sqrt{\mu}-1)t}$
exp	$\alpha\mathrm{e}^{-\alpha t}$	$\Theta(1)\,\mathrm{e}^{\alpha(\mu-1)t}$
$hyper_1$	$\dfrac{2z^2\mathrm{e}^{-\frac{2z}{z+1}\alpha t}+2\mathrm{e}^{-\frac{2}{z+1}\alpha t}}{(z+1)^2}$	$\Theta(1)\,\mathrm{e}^{\alpha t\left[\frac{(\mu-1)(1+z^2)-2z+\sqrt{(\mu^2(1+z^2)^2+(z^2-1)^2(1-2\mu)}}{(1+z)^2}\right]}$
$hyper_2$	$\dfrac{z^3\alpha\mathrm{e}^{-z\alpha t}+\alpha\mathrm{e}^{-\frac{\alpha}{z}t}}{z(z+1)}$	$\Theta(1)\,\mathrm{e}^{\alpha t\frac{(\mu-1)(1+z^2)-\mu z+\sqrt{\mu^2 z^2+(z-1)^2[\mu^2(z^2+1)-2\mu(z^2+z+1)+(z+1)^2]}}{2z}}$

Table A.3: Dominant term of $\overline{\lambda}(t)$ for different kernel shapes having the same average generation time $g = 1/\alpha$.

Specifically, we have set either $p_1/p_2 = \alpha_1/\alpha_2 = z$ (denoted by $hyper_1$) or $p_1/p_2 = \sqrt{\alpha_1/\alpha_2} = z$ (denoted by $hyper_2$). Note that in both cases the variance of the corresponding hyper-exponential distribution increases with $z \geq 1$, becoming arbitrarily large as $z \to \infty$.

For all kernel shapes, and $\mu > 1$, the growth rate of $\overline{\lambda}(t)$ is exponential, i.e., $\overline{\lambda}(t) = \Theta(e^{\eta t})$, and the same holds for $\overline{N}(t) = \int_0^t \overline{\lambda}(\tau)\,\mathrm{d}\tau$. The rate η of the exponential growth, however, depends on the specific shape.

In particular, for the two considered cases of hyper-exponential shape, η is an increasing function of z: while in the $hyper_1$ case η saturates to $2(\mu - 1)\alpha$, as $z \to \infty$, in the $hyper_2$ case η is even unbounded, as $z \to \infty$.

We also notice that the rate of the exponential kernel is larger than the rate of the Erlang-2 kernel, which is in turn larger than the rate of the deterministic kernel.

These results confirm that, even under a constant modulating function $\mu(t)$, the epidemic growth rate depends on the specific shape of the kernel function $\overline{\nu}(t)$.

Appendix B. Comparison with SEIR model

Consider a virtual disease with the following characteristics: first there is an incubation period with constant duration of 5 days, during which an exposed individual is not infectious. Then there is a disease period with constant duration

34

of 10 days, during which the infected exerts a constant infection rate.

An Hawkes process can describe exactly the considered disease using the kernel $\nu(t) = \frac{1}{10}$, $t \in (5, 15)$. Note that, similarly to what we did in Sec. 3, we normalize the kernel in such a way that $\int_0^\infty \nu(t)\,\mathrm{d}t = 1$, since we can can use $\mu(t)$ to obtain a desired reproduction number $R(t)$. Moreover, note that here the average generation time $g = \int_0^\infty t\,\nu(t)\,\mathrm{d}t$ is equal to 10 days.

If we use a SIR model, the only possibility to match the given generation time is to consider an Infectious compartment with exponential sojourn time of mean 10 days.

Within the family of compartmental models, a natural candidate to obtain a better description of the considered disease is the SEIR model, where the Exposed stage would take into account the initial (not infectious) incubation period of 5 days. Therefore, let's consider a SEIR model with an Exposed stage of mean duration 5 days, followed by an Infectious stage of mean duration 5 days, in order to match the target mean generation time. Another possible natural choice would be to take an Infectious stage of mean duration 10 days, matching the duration of the actual disease period, but notice that this would not produce the desired mean generation time.

Similarly to what we did in Sec. 3, we compare all models above in a scenario with $I_0 = 1000$ initial infections on day zero. Figure B.14 reports the mean number of people who get infected, according to SIR, Hawkes, and the two variants of SEIR, in the case of constant $\mu = 2$. The log y axes suggests that the parameter of the exponential growth differs significantly among the considered models. The SEIR models, indeed, perform better than SIR, though the one matching the correct mean generation time still overestimates the number of infected. Note that the Hawkes process does not produce any new infection during the first 5 days, as expected. The fact that the SEIR model in which the Infectious stage is exponential with mean 10 underestimates the number of infected suggests that, by a careful tuning of the sojourn time in the Infectious stage, a SEIR model could obtain the exact exponential growth rate predicted by Hawkes, though by so doing we would no longer reflect native properties of
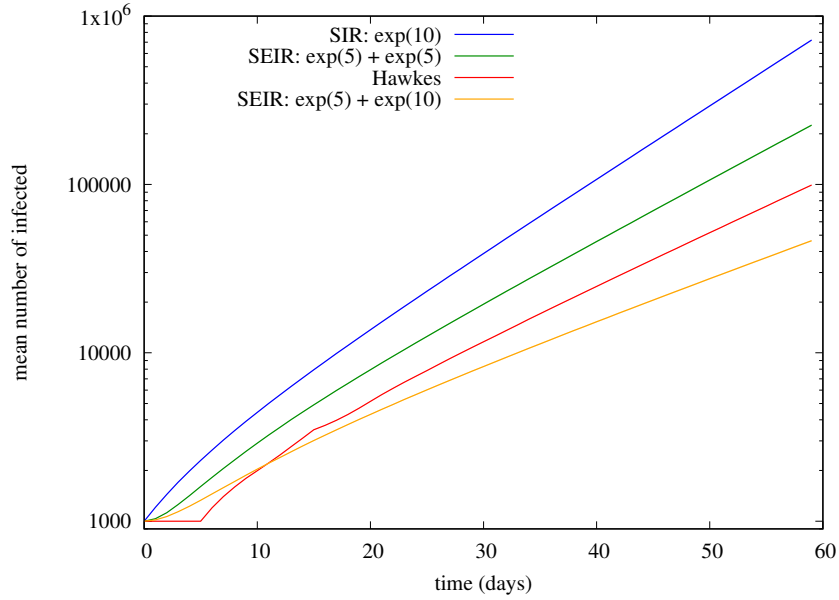
35

Figure B.14: Virtual disease with incubation period of 5 days and infectious period of 10 days. Mean number of infected individuals according to SIR, Hawkes, and two variants of SEIR, in the case of constant $\mu = 2$, $I_0 = 1000$.

the disease.

Figure B.15 shows what happens under the time-varying $\mu(t)$ already considered in Sec. 3, where the reproduction number decreases from 3 to 0.3 during the first 30 days (black curve). Again, we observe huge discrepancies among the different models, repeating the trends observed in Fig. B.14 under constant μ. Note that a SEIR model could perfectly match the actual curve predicted by the Hawkes process, since this time we could also play on the modulating function $\mu(t)$ to reproduce the behavior observed during the first days of the epidemic. However, such tuning of the SEIR model and/or of $\mu(t)$, although it would perfectly match the epidemic curve, would fail to represent true characteristics of the disease and the actual intensity of applied countermeasures, possibly producing misleading indications.
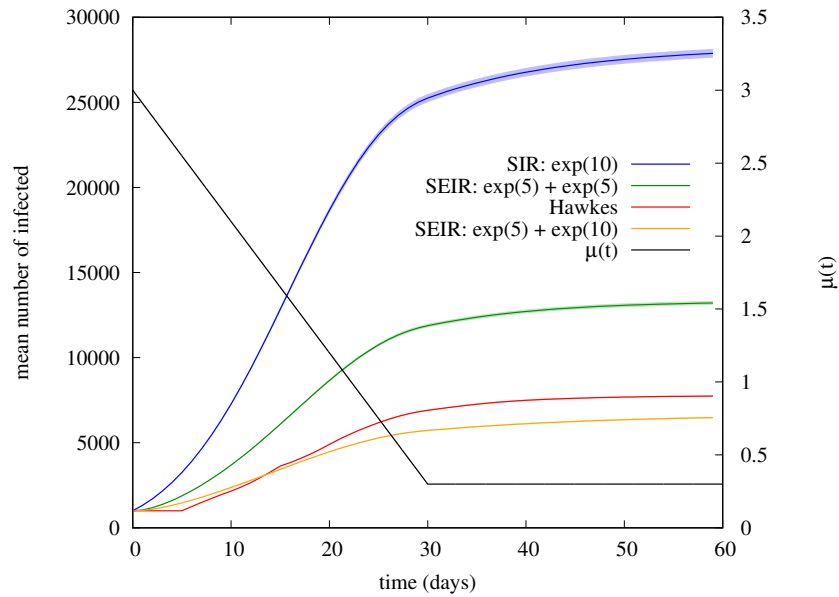
Figure B.15: Virtual disease with incubation period of 5 days and infectious period of 10 days. Mean number of infected individuals according to SIR, Hawkes, and two variants of SEIR, in the case of time-varying $\mu(t)$ (black curve), $I_0 = 1000$.

References

[1] Y. Fang, Y. Nie, M. Penny, Transmission dynamics of the COVID-19 outbreak and effectiveness of government interventions: A data-driven analysis, Journal of medical virology 92 (6) (2020) 645–659.
URL https://pubmed.ncbi.nlm.nih.gov/32141624

[2] A. J. Kucharski, T. W. Russell, C. Diamond, Y. Liu, J. Edmunds, S. Funk, R. M. Eggo, F. Sun, M. Jit, J. D. Munday, N. Davies, A. Gimma, K. van Zandvoort, H. Gibbs, J. Hellewell, C. I. Jarvis, S. Clifford, B. J. Quilty, N. I. Bosse, S. Abbott, P. Klepac, S. Flasche, Early dynamics of transmission and control of COVID-19: a mathematical modelling study, The Lancet Infectious Diseases 20 (5) (2020) 553 – 558.
URL http://www.sciencedirect.com/science/article/pii/S1473309920301444

[3] S. Pei, J. Shaman, Initial Simulation of SARS-CoV2 Spread and Intervention Effects in the Continental US, medRxiv (2020).
URL https://www.medrxiv.org/content/early/2020/03/27/2020.03.21.20040303.full.pdf

[4] D. Zou, L. Wang, P. Xu, J. Chen, W. Zhang, Q. Gu, Epidemic Model Guided Machine Learning for COVID-19 Forecasts in the United States, medRxiv (2020).
URL https://www.medrxiv.org/content/early/2020/05/25/2020.05.24.20111989.full.pdf

[5] A. C. Miller, N. J. Foti, J. A. Lewnard, N. P. Jewell, C. Guestrin, E. B. Fox, Mobility trends provide a leading indicator of changes in SARS-CoV-2 transmission, medRxiv (2020).
URL https://www.medrxiv.org/content/early/2020/05/11/2020.05.07.20094441.full.pdf

[6] C. Anastassopoulou, L. Russo, A. Tsakris, C. Siettos, Data-based analysis, modelling and forecasting of the COVID-19 outbreak, PLOS ONE 15 (3) (2020) 1–21.
URL https://doi.org/10.1371/journal.pone.0230405

[7] G. C. Calafiore, C. Novara, C. Possieri, A time-varying SIRD model for the COVID-19 contagion in Italy, Annual Reviews in Control 50 (2020) 361 – 372.
URL http://www.sciencedirect.com/science/article/pii/S1367578820300717

[8] M. Gatto, E. Bertuzzo, L. Mari, S. Miccoli, L. Carraro, R. Casagrandi, A. Rinaldo, Spread and dynamics of the COVID-19 epidemic in Italy: Effects of emergency containment measures, Proceedings of the National Academy of Sciences 117 (19) (2020) 10484–10491.
URL https://www.pnas.org/content/117/19/10484.full.pdf

[9] G. Giordano, F. Blanchini, R. Bruno, P. Colaneri, A. Di Filippo, A. Di Matteo, M. Colaneri, Modelling the COVID-19 epidemic and implementation of population-wide interventions in Italy, Nature Medicine 26 (6) (2020) 855–860.
URL https://doi.org/10.1038/s41591-020-0883-7

[10] A. G. Hawkes, Spectra of Some Self-Exciting and Mutually Exciting Point Processes, Biometrika 58 (1) (1971) 83–90.
URL http://www.jstor.org/stable/2334319

[11] A. D. Kimmel M., The Bellman-Harris Process, Branching Processes in Biology, Interdisciplinary Applied Mathematics, Springer, New York, NY 19 (2002) 87–102. doi:https://doi.org/10.1007/0-387-21639-1_5.

[12] H. Mei, J. Eisner, The Neural Hawkes Process: A Neurally Self-Modulating Multivariate Point Process, in: Proceedings of the 31st International Conference on Neural Information Processing Systems, NIPS'17, Curran Associates Inc., Red Hook, NY, USA, 2017, p. 67576767.

[13] M. Kim, D. Paini, R. Jurdak, Modeling stochastic processes in disease spread across a heterogeneous social system, Proceedings of the National Academy of Sciences 116 (2) (2019) 401–406.
URL https://www.pnas.org/content/116/2/401.full.pdf

[14] H. Xu, H. Zha, A Dirichlet Mixture Model of Hawkes Processes for Event Sequence Clustering, in: I. Guyon, U. V. Luxburg, S. Bengio, H. Wallach, R. Fergus, S. Vishwanathan, R. Garnett (Eds.), Advances in Neural Information Processing Systems, Vol. 30, Curran Associates, Inc., 2017, pp. 1354–1363.
URL https://proceedings.neurips.cc/paper/2017/file/dd8eb9f23fbd362da0e3f4e70b878c16-Paper.pdf

[15] P. Montagnon, A stochastic SIR model on a graph with epidemiological and population dynamics occurring over the same time scale, Journal of

Mathematical Biology 79 (1) (2019) 31–62.

URL https://doi.org/10.1007/s00285-019-01349-0

[16] J. D. Kelly, J. Park, R. J. Harrigan, N. A. Hoff, S. D. Lee, R. Wannier, B. Selo, M. Mossoko, B. Njoloko, E. Okitolonda-Wemakoy, P. Mbala-Kingebeni, G. W. Rutherford, T. B. Smith, S. Ahuka-Mundeke, J. J. Muyembe-Tamfum, A. W. Rimoin, F. P. Schoenberg, Real-time predictions of the 20182019 Ebola virus disease outbreak in the Democratic Republic of the Congo using Hawkes point process models, Epidemics 28 (2019) 100354.

URL   https://www.sciencedirect.com/science/article/pii/S1755436519300258

[17] G. Mohler, M. B. Short, F. Schoenberg, D. Sledge, Analyzing the Impacts of Public Policy on COVID-19 Transmission: A Case Study of the Role of Model and Dataset Selection Using Data from Indiana, Statistics and Public Policy 8 (1) (2021) 1–8.

URL https://doi.org/10.1080/2330443X.2020.1859030

[18] F. P. Schoenberg, M. Hoffmann, R. J. Harrigan, A recursive point process model for infectious diseases, Annals of the Institute of Statistical Mathematics 71 (5) (2019) 1271–1287.

URL https://doi.org/10.1007/s10463-018-0690-9

[19] A. L. Bertozzi, E. Franco, G. Mohler, M. B. Short, D. Sledge, The challenges of modeling and forecasting the spread of COVID-19, Proceedings of the National Academy of Sciences 117 (29) (2020) 16732–16738.

URL https://www.pnas.org/content/117/29/16732

[20] J. Park, A. W. Chaffee, R. J. Harrigan, F. P. Schoenberg, A non-parametric Hawkes model of the spread of Ebola in west Africa, Journal of Applied Statistics 0 (0) (2020) 1–17.

URL https://doi.org/10.1080/02664763.2020.1825646

[21] M. Akian, L. Ganassali, S. Gaubert, L. Massoulié, Probabilistic and mean-field model of COVID-19 epidemics with user mobility and contact tracing (2020). `arXiv:2009.05304`.

[22] G. N. Wong, Z. J. Weiner, A. V. Tkachenko, A. Elbanna, S. Maslov, N. Goldenfeld, Modeling COVID-19 Dynamics in Illinois under Nonpharmaceutical Interventions, Phys. Rev. X 10 (2020) 041033.
URL `https://link.aps.org/doi/10.1103/PhysRevX.10.041033`

[23] W.-H. Chiang, X. Liu, G. Mohler, Hawkes process modeling of COVID-19 with mobility leading indicators and spatial covariates, medRxiv (2020).
URL `https://www.medrxiv.org/content/early/2020/12/20/2020.06.06.20124149.full.pdf`

[24] T. Omi, N. Ueda, K. Aihara, Fully neural network based model for general temporal point processes, in: Advances in Neural Information Processing Systems, Vol. 32, Curran Associates, Inc., 2019.
URL `https://proceedings.neurips.cc/paper/2019/file/39e4973ba3321b80f37d9b55f63ed8b8-Paper.pdf`

[25] S. F. Ardabili, A. Mosavi, P. Ghamisi, F. Ferdinand, A. R. Varkonyi-Koczy, U. Reuter, T. Rabczuk, P. M. Atkinson, COVID-19 Outbreak Prediction with Machine Learning, Algorithms 13 (10) (2020).
URL `https://www.mdpi.com/1999-4893/13/10/249`

[26] M.-A. Rizoiu, S. Mishra, Q. Kong, M. Carman, L. Xie, SIR-Hawkes: Linking Epidemic Models and Hawkes Processes to Model Diffusions in Finite Populations, 2018, pp. 419–428. `doi:10.1145/3178876.3186108`.

[27] Google LLC, Google COVID-19 Community Mobility Reports, `https://www.google.com/covid19/mobility/`.

[28] Apple Inc., Apple COVID-19 Mobility Trends Reports, `https://www.apple.com/covid19/mobility`.

[29] Presidenza del Consiglio dei Ministri, Dipartimento della Protezione Civile: Italian survelliance data, `https://github.com/pcm-dpc/COVID-19`.

[30] Istat, Istituto Nazionale di Statistica, Primi risultati dell'indagine di sieroprevalenza sul SARS-CoV-2, `https://www.istat.it/it/archivio/246156`.

[31] The Incubation Period of Coronavirus Disease 2019 (COVID-19) From Publicly Reported Confirmed Cases: Estimation and Application, Annals of Internal Medicine 172 (9) (2020) 577–582, pMID: 32150748.
URL `https://doi.org/10.7326/M20-0504`

[32] N. M. Linton, T. Kobayashi, Y. Yang, K. Hayashi, A. R. Akhmetzhanov, S.-m. Jung, B. Yuan, R. Kinoshita, H. Nishiura, Incubation Period and Other Epidemiological Characteristics of 2019 Novel Coronavirus Infections with Right Truncation: A Statistical Analysis of Publicly Available Case Data, Journal of Clinical Medicine 9 (2) (2020).
URL `https://www.mdpi.com/2077-0383/9/2/538`

[33] J. Qin, C. You, Q. Lin, T. Hu, S. Yu, X.-H. Zhou, Estimation of incubation period distribution of COVID-19 using disease onset forward time: A novel cross-sectional and forward follow-up study, Science Advances 6 (33) (2020).
URL `https://advances.sciencemag.org/content/6/33/eabc1202.full.pdf`

[34] A. W. Byrne, D. McEvoy, A. B. Collins, K. Hunt, M. Casey, A. Barber, F. Butler, J. Griffin, E. A. Lane, C. McAloon, K. O'Brien, P. Wall, K. A. Walsh, S. J. More, Inferred duration of infectious period of SARS-CoV-2: rapid scoping review and analysis of available evidence for asymptomatic and symptomatic COVID-19 cases, BMJ open 10 (8) (2020) e039856–e039856, 32759252[pmid].
URL `https://pubmed.ncbi.nlm.nih.gov/32759252`

[35] J. Wallinga, P. Teunis, Different Epidemic Curves for Severe Acute Respiratory Syndrome Reveal Similar Impacts of Control Measures, American Journal of Epidemiology 160 (6) (2004) 509–516.
URL https://academic.oup.com/aje/article-pdf/160/6/509/179728/kwh255.pdf

[36] T. Obadia, R. Haneef, P.-Y. Boëlle, The R0 package: a toolbox to estimate reproduction numbers for epidemic outbreaks, BMC Medical Informatics and Decision Making 12 (1) (2012) 147. `doi:10.1186/1472-6947-12-147`.

[37] D. Cereda, M. Tirani, F. Rovida, V. Demicheli, M. Ajelli, P. Poletti, F. Trentini, G. Guzzetta, V. Marziano, A. Barone, M. Magoni, S. Deandrea, G. Diurno, M. Lombardo, M. Faccini, A. Pan, R. Bruno, E. Pariani, G. Grasselli, A. Piatti, M. Gramegna, F. Baldanti, A. Melegaro, S. Merler, The early phase of the COVID-19 outbreak in Lombardy, Italy (2020). `arXiv:2003.09320`.

[38] S. Flaxman, S. Mishra, A. Gandy, H. J. T. Unwin, T. A. Mellan, H. Coupland, C. Whittaker, H. Zhu, T. Berah, J. W. Eaton, M. Monod, P. N. Perez-Guzman, N. Schmit, L. Cilloni, K. E. C. Ainslie, M. Baguelin, A. Boonyasiri, O. Boyd, L. Cattarino, L. V. Cooper, Z. Cucunubá, G. Cuomo-Dannenburg, A. Dighe, B. Djaafara, I. Dorigatti, S. L. van Elsland, R. G. FitzJohn, K. A. M. Gaythorpe, L. Geidelberg, N. C. Grassly, W. D. Green, T. Hallett, A. Hamlet, W. Hinsley, B. Jeffrey, E. Knock, D. J. Laydon, G. Nedjati-Gilani, P. Nouvellet, K. V. Parag, I. Siveroni, H. A. Thompson, R. Verity, E. Volz, C. E. Walters, H. Wang, Y. Wang, O. J. Watson, P. Winskill, X. Xi, P. G. T. Walker, A. C. Ghani, C. A. Donnelly, S. Riley, M. A. C. Vollmer, N. M. Ferguson, L. C. Okell, S. Bhatt, I. C. C.-. R. Team, Estimating the effects of non-pharmaceutical interventions on COVID-19 in Europe, Nature 584 (7820) (2020) 257–261.
URL https://doi.org/10.1038/s41586-020-2405-7

[39] Istituto Superiore di Sanità, Characteristics of COVID-19 patients

dying in Italy, `https://www.epicentro.iss.it/en/coronavirus/`
`sars-cov-2-analysis-of-deaths`.